ELSEVIER

Thermochimica Acta 389 (2002) 109–119

thermochimica acta

www.elsevier.com/locate/tca

Catalytic effects of magnesium chromite spinel on the decomposition of lanthanum oxalate

H. Nayak, D. Bhatta*

Department of Chemistry, Utkal University, Bhubaneswar 751 004, Orissa, India

Received 19 June 2001; received in revised form 4 November 2001; accepted 12 December 2001

Abstract

A study on the thermal decomposition of mixtures of lanthanum oxalate hydrate and magnesium chromite spinel, $MgCr_2O_4$ of different molar ratios has been carried out employing thermogravimetry, differential thermal analysis, chemical analysis, infrared spectroscopy and X-ray diffraction analysis. It is evident from the data that lanthanum oxalate in the presence of mixed oxide starts to decompose at a temperature higher than the pure salt. The results reveal that chromium oxide has a retarding effect on the decomposition rate and addition of magnesium oxide leads to an observable increase in the catalytic behaviour of Cr_2O_3 towards the decomposition below 440 °C, above which it increases significantly with increasing percentage of $MgCr_2O_4$. The induced defects during the formation of solid solution alters the conductive properties of the oxide, due to generation of more holes within the catalyst, consequently increasing its, activity towards decomposition. The kinetic and thermogravimetric parameters are evaluated in the light of D_3 mechanism. The reaction occurs through three different stages and the rate constant, k is found to follow the order: stage I > stage II < stage III and LO1 > LO2 > LO3 (653–713 K), LO1 < LO2 < LO3 (713–753 K), where LO1, LO2 and LO3 stand for different mole percentage mixtures of $MgCr_2O_4$ with lanthanum oxalate.

Keywords: Lanthanum oxalate; Magnesium chromite spinel; TG; p-Type semiconductor; Catalyst effect

1. Introduction

Thermal analysis and kinetics of thermal decomposition of metal oxalates has been successfully applied to low temperature synthesis of oxides, bronzes, and high T_c superconducting precursors [1,2]. In order to make these decompositions facile many workers have reported the role of additives on it [3–5] and indicated that most active metal oxides are those of transition metals [6–9]. Metal oxalates release 'CO' as a decomposition by-product which undergoes exothermic oxidation in the presence of several transition metal oxides [10–20] and mixed oxides [21] at low temperature, there by acting as catalysts. Incorporation of rare earth elements into the lattice further increases their activity [22]. In some cases, the rare earth oxide acts as good catalytic promoters [23]. Such studies on Cr_2O_3 mixed with divalent transition metal oxide indicate that the activity is due to lattice disorder and enlargement of surface area [24]. The defect nature of the oxides results from lattice disorder and plays an important role in the catalytic efficiency with respect to the thermal decomposition of solids, especially due to their semiconducting property. Further studies on a series of transition metal oxides show that Cr_2O_3 and V_2O_5 are most active oxides when supported on another oxide [25] indicating a significant metal oxide–support interactions.

* Corresponding author.

0040-6031/02/$ – see front matter
PII: S0040-6031(02)00004-7

The present work has been carried out in hope of applying the chemistry evolved out of this study to high T_c superconducting materials [26,27].

Recent studies [28] reveal that the catalytic behaviour of multicomponent oxides and perovskites towards the oxidation. The catalytic activity of mixed oxide system [29,30] and spinels [31] are of interest due to their high selectivity. Several researchers [32,33] have studied the surface structure of solid catalysts with particular reference to the identification of the active sites which is responsible for catalytic activity. Mixed oxides of nickel and chromium are found to have posses this property due to p-type semiconductivity [34]. It has been reported [35] that the catalytic activity increases with increasing p-type semiconductivity, but according to others [36] metal oxides with high conductivity have high activity regardless of their nature n-/p-type. Moreover, p-type semiconductors, which can be converted to n-type, are effective catalysts [37].

Nickel oxide doped with chromium oxide show the largest reactivity towards the formation of $NiFe_2O_4$ which is a good catalyst [38]. The activity of nickel chromite [39] and copper oxide [40] spinels has been reported. Though studies have been carried out on a series of chromite spinel towards reduction [41] the present work has been undertaken to ascertain the catalytic activity of $MgCr_2O_4$ [42] and its effect on the oxidation of $La_2(C_2O_4)_3$. The principal objective of the study is to prepare lanthanum spinel as a by-product during the decomposition of lanthanum oxalate in the presence of $MgCr_2O_4$ spinel, which has not received much attention. The products of decomposition are characterised by chemical analysis, infrared measurement and X-ray diffraction studies.

2. Experimental

All the reagents used were of analytical grade. Pure magnesium and chromium oxides and their mixtures in the ratio (1:1) were prepared from their corresponding hydroxides and the mixed oxide spinel was prepared as reported earlier [43]. Formation of the spinel oxide was checked by XRD and IR spectroscopy.

The prepared oxides were mixed with anhydrous $La_2(C_2O_4)_3$ in different mole ratios by grinding in an agate mortar. Thermogravimetry (TG) and differential thermogravimetric studies were carried out using Schimazdu-DTG-50 thermal analyser at a heating rate of 4 °C min^{-1} in static air. The catalytic activity of the spinel on the decomposition was studied using best-fit kinetic models of solid state reactions.

3. Results and discussion

3.1. Thermal analysis

The decomposition temperatures of the lanthanum oxalate are elevated by addition of magnesium chromite, which is continued with increasing concentration of the additive. The pattern of decomposition changes significantly at higher concentration of the catalyst. The TG curves of decomposition indicate that the reaction started at around 385 °C and may result from the decomposition to $La_2O_3{\cdot}2CO_2$ intermediate, in two successive stages below, 440 °C, above which stage III starts and an oxycarbonate ($La_2O_3{\cdot}CO_2$) is supposed to be formed. The TG curves (Fig. 1) for all categories of samples were found to cross each other at 440 °C, where the formation of MgO. Cr_2O_3 types of species with spinel structures are expected to be formed, thereby catalysing the reaction. Above 440 °C the curves rise sharply depending on the concentration of the admixtures and the normal trend is reversed, i.e. rate of reaction increases with increasing additive concentration.

The DTG curves (Fig. 2), of the mixed samples have two prominent peaks. At the lowest concentration of the oxide, the peak was obtained at 388 °C, and it gradually changes to 396 °C at the highest concentration of additive. In stage III, there is a general discrepancy in the peak positions, i.e. when the concentration increases from 2 to 5 to 10%, the peak temperature, T_m, changes from 440 to 458 to 452 °C. Moreover, the symmetry of the DTG peaks of stage III is exactly reverse of the previous stages, during the decomposition.

3.2. Spectral analysis

The IR spectra (Fig. 3) of the oxalate samples mixed with magnesium chromite shows signals at 1615 and 1315 cm^{-1} corresponding to oxalate ion. The presence of absorption bands at 795 and 496 cm^{-1} may be due to –M–O (M = La) stretching in $La_2(C_2O_4)_3$. But no

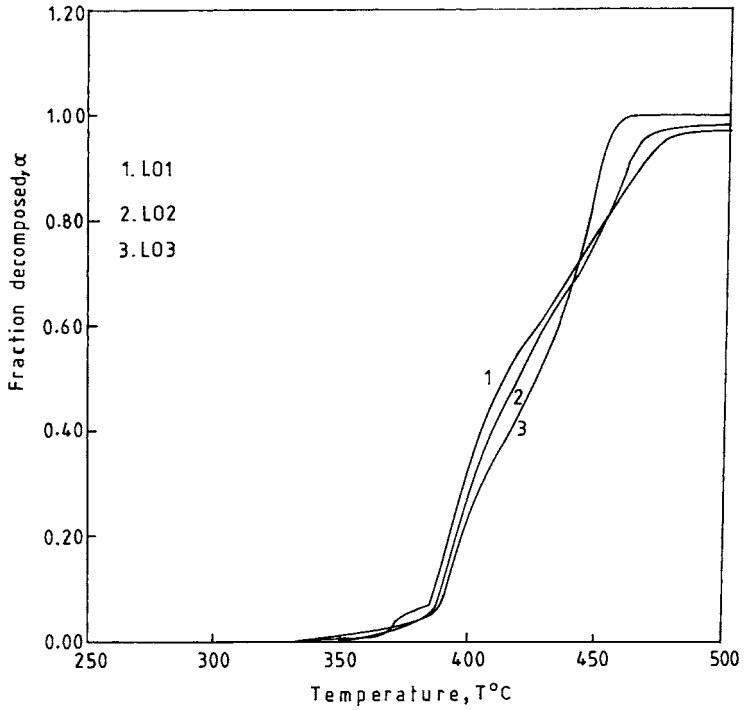

Fig. 1. Variation of the fraction of decomposition α with temperature T for $La_2(C_2O_4)_3$ and $MgCr_2O_4$ mixture at different mole percentages of LO1, $La_2(C_2O) + MgCr_2O_4$ (2 mol%); LO2, $La_2(C_2O_4)_3 + MgCr_2O_4$ (5 mol%) and LO3, $La_2(C_2O_4)_3 + MgCr_2O_4$ (10 mol%).

prominent bands are obtained for the spinel oxides indicating that the –M–O bonds are not well defined and thought to have some ionic character.

The IR spectra of the decomposition product after heating at 500 °C shows a prominent peak at 1363 cm^{-1} which may be due to the formation of carbonate, but the product shows no peak for –M–O stretching probably due to the formation of lanthanum spinel oxides which is an ionic solid with high crystal defects.

3.3. XRD analysis of prepared $MgCr_2O_4$

X-ray diffraction pattern (Fig. 4) of $MgCr_2O_4$ shows peaks at d-values of 4.81, 2.52 and 1.61 Å corresponding to true and uniphase spinel structure (Table 1), but the intensities are comparatively less due to incomplete formation of spinel. Additional peaks at d-values of 2.11 and 1.49 Å are obtained indicating the presence of residual MgO in the sample existing in the form of $MgO{\cdot}Cr_2O_3$ during heating. Moreover, peaks corresponding to Cr_2O_3 underwent shift to lower 2θ angle at d-values of 3.19 Å as against the value of 3.63 Å for pure Cr_2O_3. This confirms the formation of solid solution of the oxides. The peak at $d = 2.69$ Å may be due to the presence of residual Cr_2O_3 due to incomplete reaction.

3.4. Kinetic analysis

The thermogravimetric data are analysed and the fractional decomposition, α are plotted against temperature T (Fig. 5) for different categories of materials. The plots were also drawn for the mixture with different concentrations of the spinel (Fig. 1). It is evident from the data that MgO, being an insulator oxide has no much catalytic activity on the decomposition process, but Cr_2O_3 retards the reaction. $MgCr_2O_4$ has some pragmatic effect at 380–440 °C and it retards the rate (effect is less than Cr_2O_3) and at higher temperature it increases the rate significantly. Completion of the reaction takes place without any slow stage (Table 2).

Plots $d\alpha/dT$ vs. T (Fig. 2) were made for each mixture. Double peak exotherms were obtained confirming that

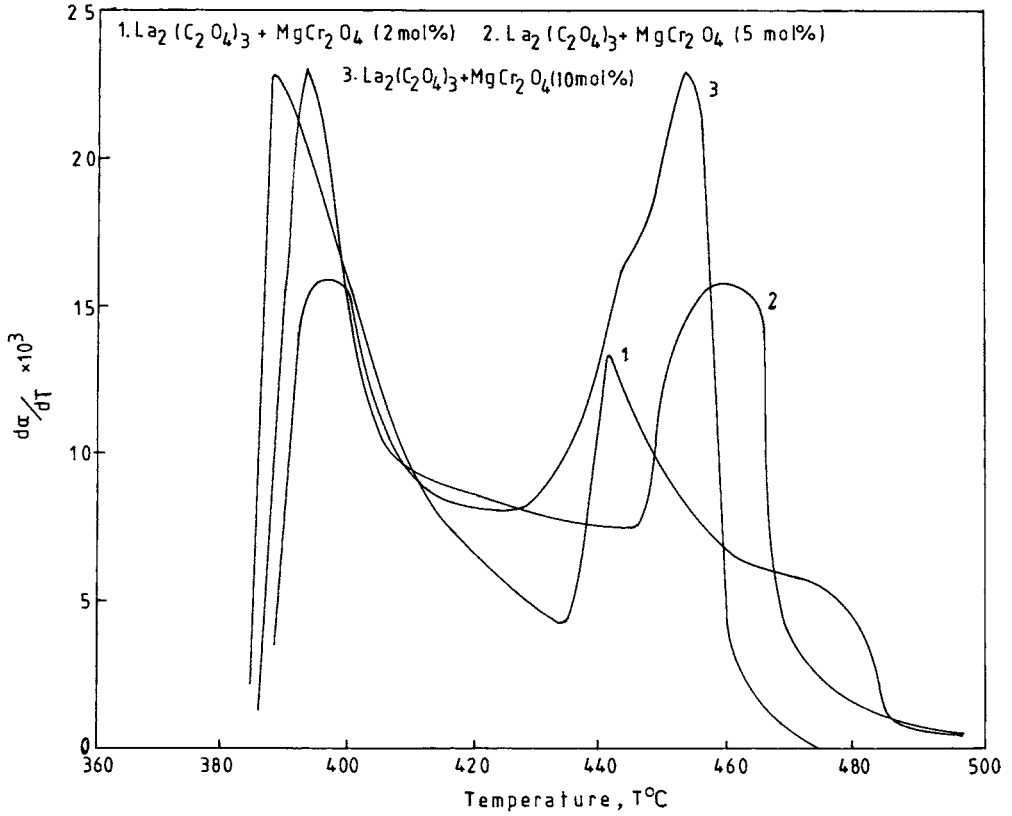

Fig. 2. Differential thermogravimetric curves for $La_2(C_2O_4)_3$ and $MgCr_2O_4$ mixture at different mole percentages.

decomposition took place in two major steps at two different temperature regions. The first step was a double stage process having one acceleratory (stage 1) and an slow (stage II) rate of decomposition, but stage III is totally acceleratory one (Fig. 1). During the last stage (second step), the action of the spinel becomes dominant, which increases with increasing concentration of the spinel. The shape of the DTG curve change with ($\Delta L_O T/\Delta H_i T$) ratio, <1 to >1, as the spinel concentration increases from 2 to 10 mol%, i.e. at higher concentration of the oxide, the mechanism became diffusion controlled ($\Delta L_O T/\Delta H_i T > 1$) and $(d\alpha/dT)_{max}$ varies between 0.01 and 0.04 and $0.7 < \alpha_{max} < 0.85$.

The kinetic parameters for the important stages of decomposition were determined using Coat–Redfern's equation

$$\log \frac{g(\alpha)}{T^2} = \log \frac{AR}{\beta E} - \frac{E}{2.303RT} \quad (1)$$

where A is the pre-exponential factor, β the heating rate, E the energy of activation, R the universal gas constant and T the absolute temperature. The log $g(\alpha)/T^2$ is calculated for each possible rate controlling mechanism using various solid state reaction models and plotted against $1/T$ (Fig. 6), using the best-fit model for separate stages of reaction. The value of $g(\alpha)$ with highest coefficient of linear regression analysis (r) gives the idea regarding the best-fit mechanism (Table 3). Values of $g(\alpha)$ were chosen which corresponded with the best-fitting model F_3 in the temperature region 380–440 °C; beyond which the mechanism switched over to a three-dimensional diffusion type (D_3). However, the data was analysed in the light of D_3 mechanism over the entire temperature range, 380–480 °C, in order to compare all the data.

The values of the activation energy, E and frequency factor A were calculated (Table 4), respectively, from the slopes and intercepts of the Coat–Redfern plot for each sample which indicate three different stages in

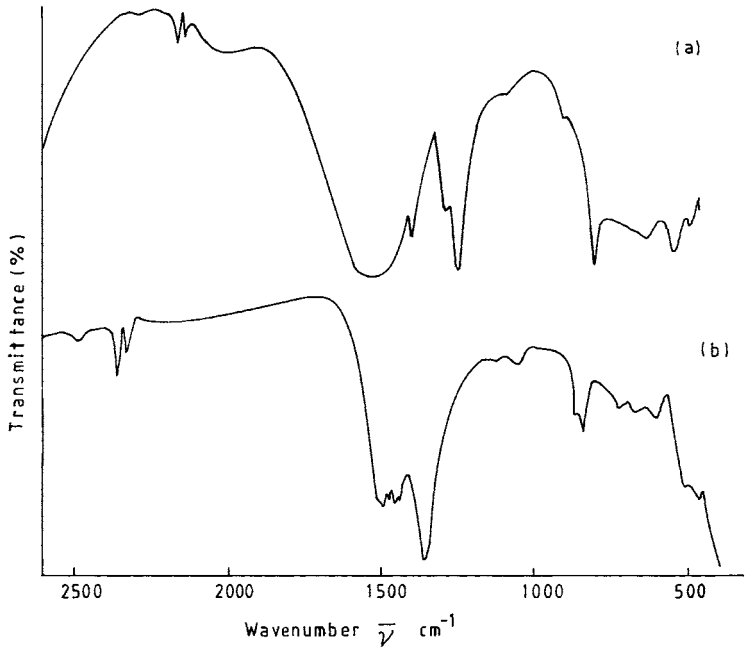

Fig. 3. Infrared spectra for the mixture of lanthanum oxalate and magnesium chromite determined at room temperature.

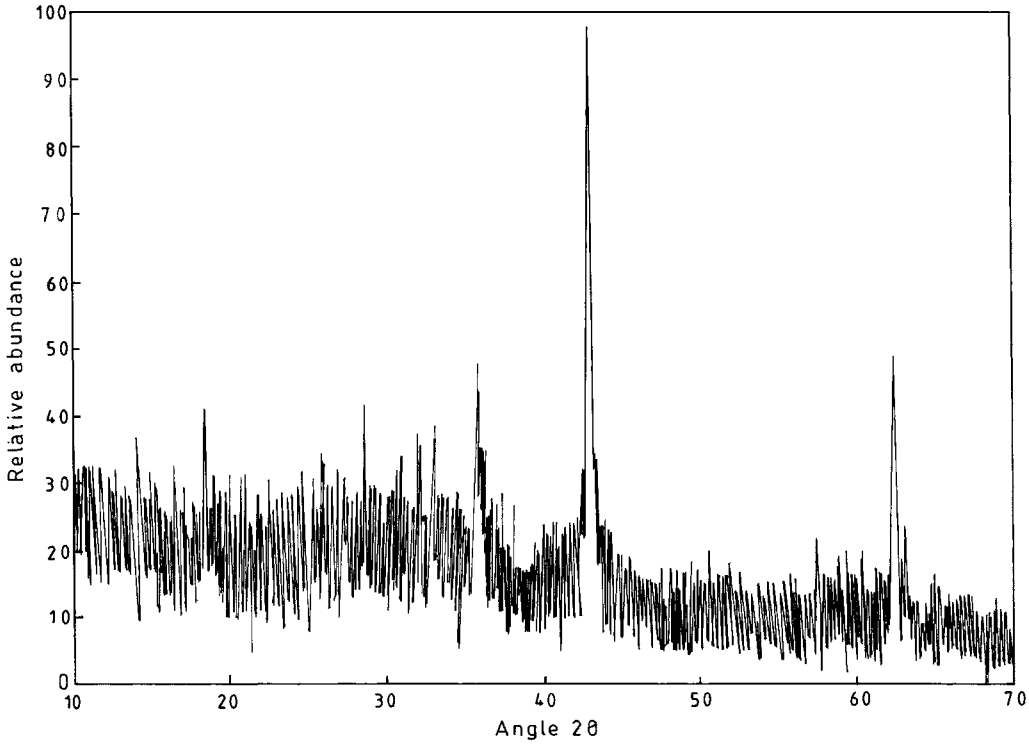

Fig. 4. X-ray diffraction pattern for magnesium chromite spinel.

Table 1
XRD data of $MgCr_2O_4$ oxide catalyst

Samples	d (Å)
Cr_2O_3	3.63
	2.67
	2.48
	2.18
	1.82
	1.67
	1.47
	1.43
$MgCr_2O_4$	4.8076
	3.1947
	2.6951
	2.5209
	2.1139
	1.606
	1.4913
MgO	2.43
	2.11
	1.49
	1.27
	1.22
	1.05
	0.94
	0.86

Table 2
Fractional decomposition, α for catalysed and uncatalysed reactions at different temperatures, with percentage of mass loss[a]

T (K)	α				Loss			
	LO	LO1	LO2	LO3	LO	LO1	LO2	LO3
653	0.05	0.064	0.044	0.040	1.82	2.0	1.40	1.11
673	0.364	0.327	0.275	0.225	13.47	10.30	8.61	6.44
623	0.557	0.546	0.500	0.431	20.60	17.22	15.66	12.34
713	0.674	0.682	0.666	0.651	24.93	21.50	20.85	18.65
733	0.787	0.846	0.862	0.986	29.11	26.70	27.0	28.25
753	0.841	0.959	0.956	0.998	31.12	30.23	30.0	28.6

[a] LO, LO1, LO2 and LO3 stand for $La_2(C_2O_4)$ (pure), $La_2(C_2O_4)_3 + MgCr_2O_4$ (2 mol%), $La_2(C_2O_4)_3 + MgCr_2O_4$ (5 mol%) and $La_2(C_2O_4)_3 + MgCr_2O_4$ (10 mol%), respectively.

the decomposition. The most plausible mechanism and the corresponding kinetics and thermodynamic parameters with correlation coefficients for different materials are all listed in Table 2, using the equations [44]

$$\Delta H^* = E - RT \tag{2}$$

$$\Delta S^* = R\left(\ln \frac{hA}{k_B T} - 1\right) \tag{3}$$

$$\Delta G^* = \Delta H^* - T\Delta S^* \tag{4}$$

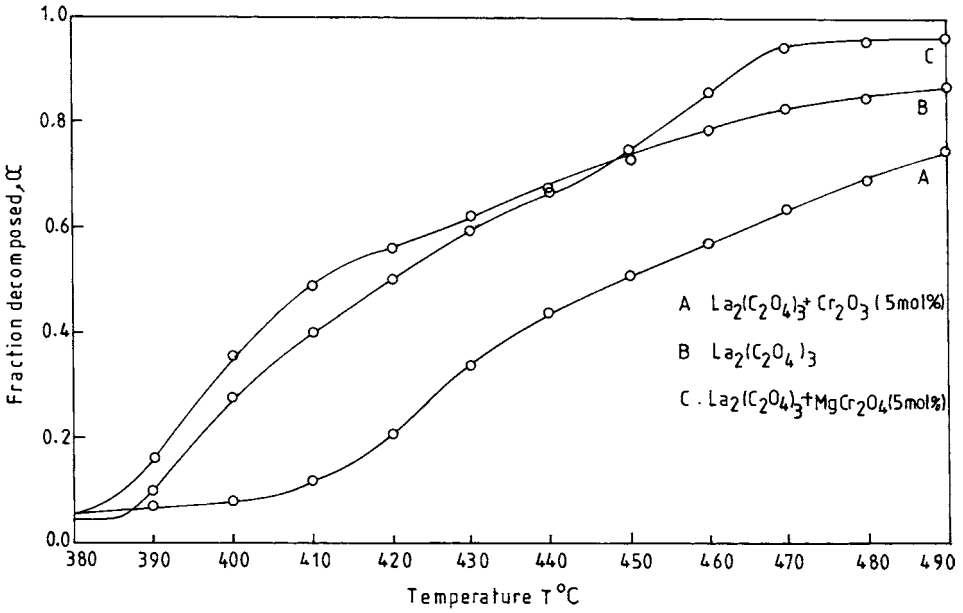

Fig. 5. Variation of α with T for different categories of lanthanum oxalate samples.

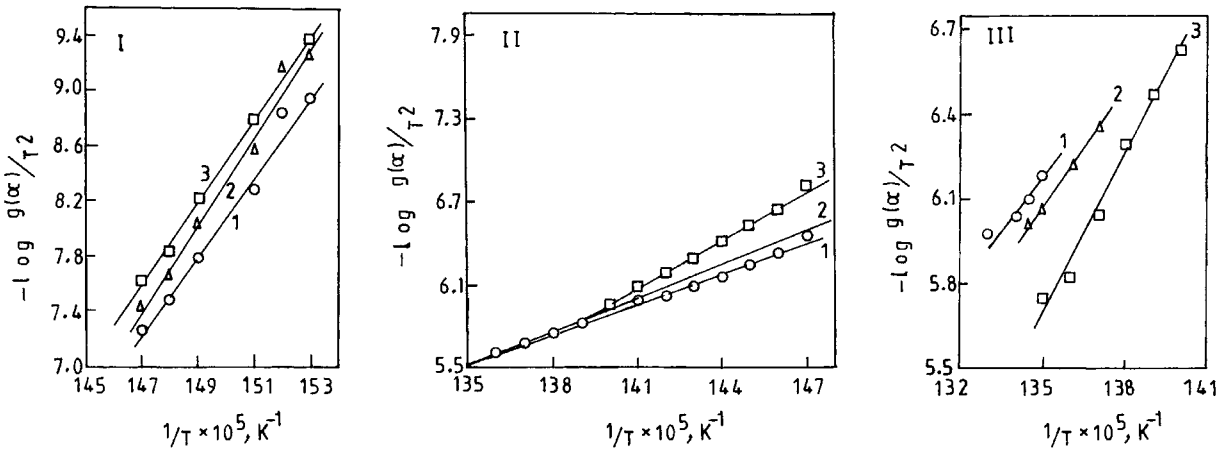

Fig. 6. Variation of $\log g(\alpha)/T^2$ with $1/T$ for the D_3 mechanism determined from Coat–Redfern's equation for different categories of mixtures at three different stages of reactions and different temperatures region.

Table 3
Determination of best-fit mechanism using various possible rate determining integral functions, $g(\alpha)$

Mechanism	Functions, $g(\alpha)$	Correlation coefficient, r	
		653–713 K	713–743 K
(1) Diffusion controlled			
Three-dimensional, D_3	$[1-(1-\alpha)^{1/3}]^2$	0.9672	0.9998
Two-dimensional, D_2	$(1-\alpha)\ln(1-\alpha)+\alpha$	0.9722	0.9972
One-dimensional, D_1	α^2	0.9814	0.9869
(2) Order of reaction			
Third order, F_3	$[1/(1-\alpha)]^2$	0.9996	0.9749
Second order, F_2	$1/1-\alpha$	0.9924	0.9762
First order, F_1	$-\ln(1-\alpha)$	0.9867	0.9645

Table 4
Determination of Arrhenius and thermodynamic parameters for the decomposition of various samples using D_3 mechanism

Samples	Stages of reaction	T_s (K)	E (kJ mol^{-1})	$\ln(A)$ (min^{-1})	ΔS (J mol^{-1} K^{-1})	ΔH (kJ mol^{-1})	ΔG (kJ mol^{-1})
LO1	Stage I, 653–678 K	672	567.35	96.285	540.53	562.26	199.03
	Stage II, 678–738 K	713	141.30	19.51	−98.29	135.37	205.45
	Stage III, 738–753 K	738	193.33	28.30	−25.42	187.195	206.00
LO2	Stage I, 653–678 K	668	628.85	106.83	628.25	623.31	204.89
	Stage II, 678–728 K	724	169.84	24.39	−57.79	163.82	205.66
	Stage III, 728–743 K	732	260.14	39.65	68.97	254.06	203.97
LO3	Stage I, 653–678 K	670	585.42	98.58	559.61	579.85	204.92
	Stage II, 678–713 K	713	225.53	34.01	22.31	219.60	203.69
	Stage III, 713–743 K	726	337.65	53.28	182.32	331.61	199.24

ΔH^*, ΔS^* and ΔG^* are the enthalpy, entropy and free energy changes of activation, respectively; h is the Planck constant and k_B the Boltzmann constant. An interesting phenomenon observed was that addition of spinel decreased the fraction, α as well as the rate of reaction. At the highest concentration of the admixture, the slowest rates were observed. Addition of Cr_2O_3 to MgO decreased the reaction rate which may be due to decrease in the catalytic activity as the decomposition progressed and reduction in the flux of oxalate ions adsorbed on the catalyst surface [45]. Although Cr_2O_3 is a p-type semiconductor, it shows high electrical conductivity with partial or complete electron transfer. As a result there is an apparently irreversible changes in the oxidation state of the metal ion due to the formation of chromate [46] ($Cr_2O_3 - CrO_4^{2-}$) during the process.

The retardation of the reaction rate was up to 440 °C above which there was an appreciable increase in rate. The rate was acceleratory throughout almost to completion, which may be due to the formation of Mg–Cr solid solution resulting $MgCr_2O_4$, a p-type semiconductor [49].

Discussing the rate constant for different samples in the light of D_3 mechanism it was found that $k_{\text{stage I}} > k_{\text{stage II}} < k_{\text{stage III}}$, for all the samples but the $k_{\text{stage II}}$ became much less in comparison to $k_{\text{stage III}}$ at the highest concentration of spinel (Table 5). With rising temperature the numerical value of k were compared for different samples by taking the values at constant temperature in order to avoid the effects of temperature on the reaction rate, i.e. for 10 mol% mixture of $MgCr_2O_4$ in $La_2(C_2O_4)_3$ though $k_{\text{stage I}}$ was less than $k_{\text{stage II}}$, the rates were determined at 395 and 415 °C, respectively. In order to compare the data the temperature is fixed at 395 °C for the fixed values of E and A and it was found that $k_{\text{stage I}} > k_{\text{stage II}}$. The decrease in values of k took place due to changes in activation energy and pre-exponential factor during the second stage.

Table 5
Rate constants for different stages of decomposition of various samples determined at various temperatures

Sample	Rate constant, k ($\times 10^3$ s^{-1})[a]		
	Stage I	Stage II	Stage III
LO1	2.57 (395 °C) 50.34 (415 °C)	5.55 (415 °C) 18.33 (450 °C)	20.99 (450 °C)
LO2	1.66 (395 °C) 44.57 (415 °C)	3.93 (415 °C) 21.08 (450 °C)	26.63 (450 °C)
LO3	1.08 (395 °C) 23.06 (415 °C)	5.91 (415 °C) 30.02 (450 °C)	55.4 (450 °C)

[a] Figures in the bracket indicate temperature.

The activation energy of all types of sample was independent of temperature and followed the same trend as that of the rate constant. It was lower in the case of pure lanthanum oxalate than that of the mixture in all the stages between 380 and 480 °C. The increase in the values of E in case of mixture may be attributed to encapsulation taking place due to oxidation of Cr_2O_3 to CrO_4^{2-}, which adsorbed on the surface of the target material. But once the encapsulation broke, the reaction proceeds spontaneously with lower activation energy (stage II). The value again increase in stage III due to a complex mechanism, during which solid solution of La^{3+} was supposed to be formed with the spinel so that additional energy was required for electron transfer to take place. Activation energy for different materials followed the increasing order with increasing concentration of the additive.

3.5. Role of spinel and mechanism of decomposition

Chromium trioxide acts as a negative catalyst for the decomposition of lanthanum oxalate, whereas the increase in catalytic activity after the formation of chromite spinel is due to dissolution of Mg^{2+} ion in the Cr_2O_3 lattice as proposed by earlier workers [48]. This dissolution may occur in cationic vacancies, in interstitial positions or by substitution of Cr^{3+} ion in Cr_2O_3 by Mg^{2+}. Cr_2O_3 is a p-type semiconductor and by valence induction with stable charged $Mg^{2+}O^{2-}$, forms spinel having structure $(Cr_{2-2x}{}^{3+}Cr_x{}^{4+}Mg_x{}^{2+}/\boxed{+})O_3{}^{2-}$ at the point of inflection at 440 °C, where $\boxed{+}$ is the Ree's notation for cation vacancy. The reaction is diffusion controlled which takes place through the layers of products. The $MgCr_2O_4$ reacts with $La_2O_3{\cdot}2CO_2$ formed from stage II resulting partly in $(Mg_x{}^{2+}La_{1-x}{}^{3+})$, $(Cr_{1-x}{}^{3+}Cr_x{}^{4+})O_3{}^{2-}$ and partly $(Cr_{2-2x}{}^{3+}Cr_x{}^{4+}Mg_x{}^{2+}/\boxed{+})O_3{}^{2-}$ type of species. The thickness of these continuously increases during the process. Under the experimental conditions, the Cr^{4+} diffuses to the surface of $C_2O_4{}^{2-}$ ion at a rate immeasurably less than the rate of the chemical reaction

between $C_2O_4^{2-}$ and Cr^{4+} to form CO_2 at lower concentration of the $MgCr_2O_4$ as

$$C_2O_4^{2-} + 2Cr^{4+} \rightleftharpoons 2CO_2 + 2Cr^{3+} \quad \text{(i)}$$

which becomes fast with increasing concentration of $MgCr_2O_4$. The relationship evolved by Jander (D_3) has been extensively used over a wide degree of conversion. The diffusion kinetics of the reaction in solids is valid for particles of any shape [47]. At the point of inflection it is supposed that carbonate decomposition takes place, as $(Mg_x^{2+}La_{1-x}^{3+})$, $(Cr_{1-x}^{3+}Cr_x^{4+})O_3^{2-}$ is a p-type semiconductor and promotes the reaction as

$$CO_3^{2-} + Cr^{4+} \rightleftharpoons Cr^{3+} + CO_3^{-} \quad \text{(ii)}$$

$$2CO_3^{-} \rightleftharpoons 2CO_2 + O_2^{-} \quad \text{(iii)}$$

$$2La^{3+} + \tfrac{3}{2}O_2^{2-} + CO_2 \rightleftharpoons La_2O_3 \cdot CO_2 \quad \text{(iv)}$$

The cation Cr^{3+} can take up a hole, p^+ with the inverse transfer [48] and the group thus becomes $Cr^{3+}p^+$ or Cr^{4+}. Thus the reaction rate of the catalysed process appears to be a function of the semiconducting properties of $MgCr_2O_4$ spinel catalyst.

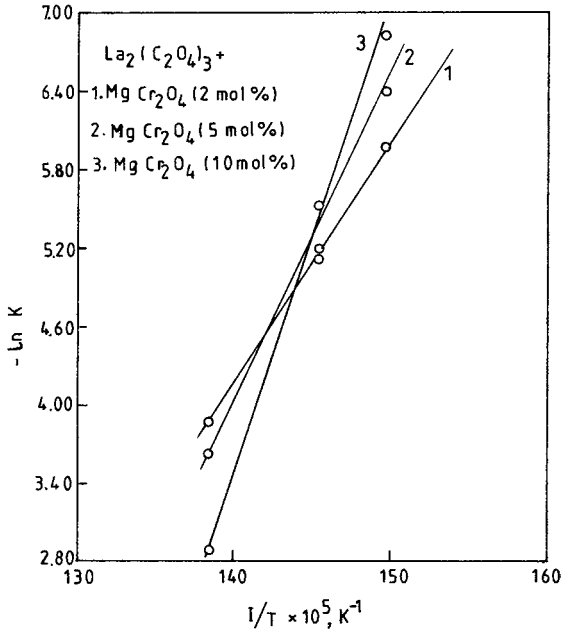

Fig. 7. Arrhenius plots $-\ln k$ vs. $1/T$ for $La_2(C_2O_4)_3$ and $MgCr_2O_4$ mixture for three different mole percentages of the latter.

3.6. Kinetic compensation effect

The Arrhenius plot (Fig. 7) for different categories of samples for each stage of reaction shows the existence of a kinetic behaviour [49] hence the kinetic compensation law is established within the group of related heterogeneous catalyses. Compensation plots (Fig. 8) are obtained in terms of $g(\alpha)$ for the individual members of a set of related rate processes. Data on compensation parameter B and e together with the correlation coefficient of linear regression analysis has been given in Table 6, using isokinetic relation:

$$\ln A = B + eE \quad (5)$$

the above equation can be used to review the similarity inherent, in obedience to control through common features in the reaction mechanism for each stage of the reaction. Compensation law is applied because all the decomposition of the set proceed in very similar

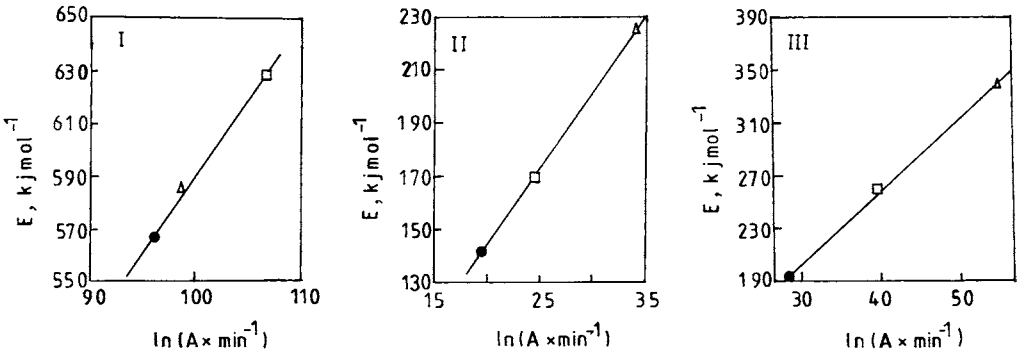

Fig. 8. Verification of compensation law for different categories of mixtures of different stages in the reactions: LO1 (●); LO2 (□) and LO3 (△).

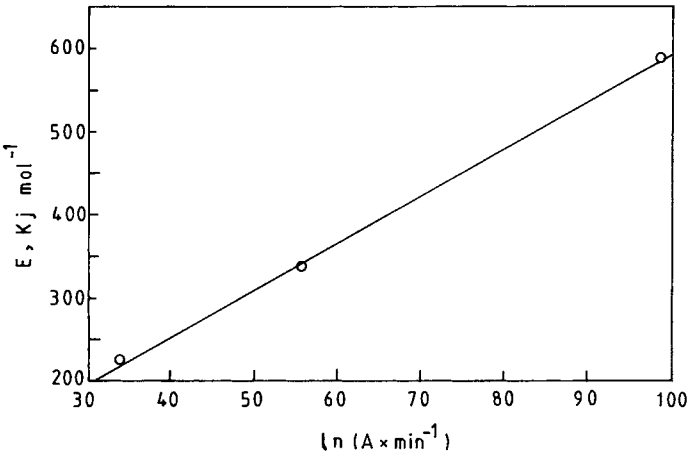

Fig. 9. Verification of compensation law for sample LO3 undergoing a change of mechanism from stages I to III.

Table 6
Derivation of compensation parameters using D_3 mechanism in Coat–Redfern's equation for each stage in different samples

Stages of reaction	Best-fit mechanism	Compensation parameters		r
		$-B$	e	
I	D_3	3.281	0.1749	0.9967
II	D_3	4.48	0.1722	0.9999
III	D_3	5.254	0.1732	0.9999

temperature interval and is ascribed to the kinetic consistency of rate processes, which involve rupture of bonds of similar strength in comparable reactants and measured within similar temperature interval [50,51].

The compensation behaviour is also set to occur when a solid state decomposition exhibits changes in mechanism [52,53] as indicated in Fig. 9. The point, at which there is change in slopes of the Arrhenius plot, is the isokinetic temperature for the two different rate processes. The mechanism is F_3 for stages I and II, but changes to D_3 in stage III. The e characterises the strength of the bond which has broken when gaseous products are formed, suggesting identical bond scission during the process, but B is related [50,54] to the structure and defects in the starting material or to the mobility of constituents of the crystal lattice which is highest in stage III, showing larger defects due to the formation of solid solutions.

Acknowledgements

Author H. Nayak thanks CSIR, New Delhi, for providing research fellowship to carry out the work.

References

[1] Y. Saikali, Thermochim. Acta 106 (1986) 1.
[2] C.T. Wang, J.L.S. Lin, J.H. Lin, Y.J. Su, S.J. Yang, S.C. Hsu, Mater. Res. Soc. Symp. Proc. 99 (1988) 257.
[3] N. Routra, D. Bhatta, J. Therm. Anal. 51 (1998) 585.
[4] S. Bose, S. Bhatta, D. Bhatta, Radiat. Eff. Def. Solids 145 (1998) 263.
[5] S. Bose, K.K. Sahu, D. Bhatta, Indian J. Chem. A 33 (1994) 230.
[6] W.K. Rudloff, E.S. Freeman, J. Therm. Anal. 18 (1980) 359.
[7] T. Wydeven, J. Catal. 19 (1970) 162.
[8] J. Joseph, T.D.R. Nair, J. Therm. Anal. 14 (1978) 271.
[9] N. Routra, D. Bhatta, Indian J. Chem. A 38 (1999) 1047.
[10] R. Majumdar, P. Sarkar, U. Ray, M. Roy Mukhopadhyay, Thermochim. Acta 335 (1999) 43.
[11] M. Shelef, K. Otto, H. Gandhi, J. Catal. 12 (1968) 12.
[12] Y. Yao, J. Catal. 33 (1974) 108.
[13] M. Harutta, S. Tsubotta, T. Kobayashi, H. Kageyama, M.J. Genet, B. Delmon, J. Catal. 144 (1993) 175.
[14] N. Yamada, M. Harutta, J. Koyabashi, S. Iijima, J. Catal. 115 (1989) 301.
[15] D.A.H. Cunningham, T. Koyabashi, N. Kamijo, M. Haruta, Catal. Lett. 25 (1994) 257.
[16] M. Meng, P. Lin, Y. Fu, Catal. Lett. 48 (1997) 213.
[17] Y.J. Mergler, A. Van Aalst, J. Van Delft, B.E. Niewenhuys, Stud. Surf. Sci. Catal. 96 (1995) 163.
[18] Y.J. Mergler, A. Van Aalst, J. Van Delft, B.E. Niewenhuys, Appl. Catal. B 10 (1996) 245.

[19] Y.J. Mergler, J. Hoebink, B.E. Niewenhuys, J. Catal. 167 (1997) 305.
[20] J. Jansson, J. Catal. 194 (2000) 55.
[21] L.S. Pukhaber, H. Cheung, D.L. Cocke, A. Clearfield, Solid State Ionics 32–33 (1989) 206.
[22] A.J. Dyakonov, D.A. Grider, B.J. McCormick, P.K. Kohol, Appl. Catal. 192 (2000) 235.
[23] J. Petryk, E. Kolakowska, Appl. Catal. B 24 (2000) 121.
[24] S. Ohyama, H. Kishida, Appl. Catal. 172 (1998) 241.
[25] S. Krishnamurty, J.A. Rivas, M.D. Amridis, J. Catal. 193 (2000) 264.
[26] C.N.R. Rao, R. Vijayaraghaban, L. Granapathy, S.V. Bhatta, J. Solid State Chem. 79 (1989) 177.
[27] I.K. Gopalkrishnan, P.V.P.S.S. Sastry, G.M. Pathak, J.V. Yakhmi, R.M. Iyer, A. Sequeira, H. Rajgopal, TMS Vol. High Temperature Superconductivity Oxides, 1989.
[28] V.C. Belessi, C.N. Costa, T.V. Bakas, T. Anastasiadou, P.J. Pomonis, A.M. Etstathiou, Catal. Today 59 (2000) 347.
[29] R.K. Grasselli, J.D. Burrington, Adv. Catal. 30 (1981) 133.
[30] J.A. Rabo, in: Zeolite Chemistry and Catalysis, ACS Monograph No. 171, American Chemical Society, Washington, DC, 1976.
[31] B.N. Dolgov, Catalysis in Organic Chemistry, GkhI, M 1959.
[32] F. Solymosi, E. Krix, J. Catal. 1 (1962) 468.
[33] A.A. Said, J. Therm. Anal. 37 (1991) 959.
[34] K.J. Haralambous, Z. Loizos, N. Spyrellis, Mater. Lett. 11 (3–4) (1991) 133.
[35] I.W. Collins, Inorg. Chim. Acta 39 (1980) 53.
[36] M. Shimokawabe, R. Furuichi, T. Ishii, Thermochim. Acta 20 (1997) 347.
[37] A.A. Said, E.A. Hassan, K.M. Abd Et. Salaam, Surf. Technol. 20 (2) (1983) 131.
[38] J.H. De Boer (Ed.), Reactivity of Solids, Elsevier, Amsterdam, 1961, p. 409.
[39] M.R. Udupa, Thermochim. Acta 13 (1975) 349.
[40] A.A. Said, R.A. Qalmi, Thermochim. Acta 275 (1986) 83.
[41] J. Sloczynski, J. Janas, T. Machej, J. Rynkowski, J. Stoch, Appl. Catal. 24 (2000) 45.
[42] G. Huttig, H. Kittel, Z. Anorg. Chem. 217 (1934) 194.
[43] H. Bamford, C.F.H. Tipper (Eds.), Comprehensive Chemical Kinetics, Vol. 22, Reaction in Solids, Elsevier, Amsterdam, 1980, p. 269.
[44] J. Straszko, M. Olszak-Humienik, J. Mozejko, J. Therm. Anal. 59 (3) (2000) 935.
[45] S.R. Mohanty, M.N. Ray, Indian J. Chem. 7 (1969) 264.
[46] D. Bhatta, M.K. Sahoo, S. Mishra, Thermochim. Acta 180 (1991) 155.
[47] P.P. Budnikov, A.M. Ginstlings, in: Principle of Solid State Chemistry Reaction in Solids, Mcraten and Sons Ltd., London, 1968, p. 308.
[48] J.P. Suchet, Chemical Physics of Semiconductors, Van Nostrand, London, 1965.
[49] A.K. Galwey, Thermochim. Acta 294 (1997) 205.
[50] J. Zsako, Cs. Varhelyi, G. Liptay, K. Szilagyi, J. Therm. Anal. 7 (1975) 41.
[51] J. Zsako, Cs. Varhely, B. Csegedi, Thermochim. Acta 45 (1981) 11.
[52] M.C. Ball, L. Portwood, J. Therm. Anal. 41 (1994) 347.
[53] M.C. Ball, Thermochim. Acta 257 (1995) 139.
[54] A.I. Lesnikovich, V.A. Levchik, J. Therm. Anal. 30 (1985) 677.